Efficient green electrophosphorescence based on ambipolar nonconjugated polymers: Evaluation of transport and emission properties

S. A. Bagnich,[1] Th. Unger,[1] F. Jaiser,[1] D. Neher,[1,a)] M. W. Thesen,[2] and H. Krueger[2]
[1]*Physik weicher Materie, Universität Potsdam, Karl-Liebknecht-Str. 24-25, Potsdam-Golm 14476, Germany*
[2]*Fraunhofer-Institute for Applied Polymer Research, Geiselbergstr. 69, Potsdam-Golm 14476, Germany*

(Received 17 May 2011; accepted 17 June 2011; published online 15 August 2011)

New materials for polymer organic light-emitting diodes based on a polymer matrix doped with phosphorescent dyes are presented. The matrix system is based on a polystyrene backbone bearing either electron or hole transporting units at the 4-position of each repeat unit. Random copolymers and polymer blend systems of the homopolymers are prepared, both with 62 wt.% electron transporting and 38 wt.% hole transporting moieties. Adding a green electrophosphorescent dye to the polymer matrix leads to efficient electroluminescence with a maximum current efficiency of 35 cd/A and a maximum external quantum efficiency of up to 10%. The mobilities of electrons and holes in the dye-doped copolymer, as measured by transient electroluminescence, are around 5×10^{-5} and 5×10^{-6} cm^2/Vs, respectively, while the blend of the two homopolymers exhibits slightly lower mobilities of both types of carriers. Despite the pronounced imbalance of charge transport, the device performance is almost entirely limited by the phosphorescence efficiency of the dye, implying balanced flow of holes and electrons into the active region. Also, devices made with either the copolymer or the blend yielded very similar device efficiencies, despite the noticeable difference in electron and hole mobility. It is proposed that electrons are efficiently blocked at the interlayer and that the so-formed space charge assists the balanced injection of holes. © *2011 American Institute of Physics*. [doi:10.1063/1.3618681]

I. INTRODUCTION

During the past two decades, polymeric organic light-emitting diodes (PLEDs) have attracted continuous attention because of the possibility for light-weight, low-cost, paper-thin flexible display and lighting applications. At first, most polymer light-emitting diodes were fluorescent.[1] The internal quantum efficiency of these fluorescent organic light-emitting diodes (OLEDs) was limited to 25%, due to spin-symmetry conservation.[2] In the mid–nineties, the concept of electrophosphorescence was introduced into OLEDs.[3,4] Here, emitters comprising a heavy metal atom with strong spin-orbit coupling, which enhances intersystem crossing, were incorporated in the emission layers. The first phosphorescent OLEDs utilized small molecules,[5,6] but later a number of groups fabricated polymer-based electrophosphorescent devices (PPLEDs), combining the virtues of the high efficiency of electrophosphorescence with easy fabrication of polymer light-emitting devices.[7–12] Both mixtures of host polymers with phosphorescent small molecules[7,8,10] and phosphorescent polymers[11,12] have been used as the emitting layer in such devices.

Emission layers (EMLs) comprising solely the electrophosphorescent dyes have been shown to be inefficient in most cases. This phenomenon has been attributed to the annihilation of the long-lived triplet excitons on adjacent dye molecules (triplet-triplet-annihilation). The most efficient electrophosphorescent devices therefore use multi-component EMLs, which have the dye incorporated (physically or chemically) into a charge-transporting matrix. Here, excitation of the dye proceeds either by direct charge trapping or by the harvesting of singlet and triplet excitons formed on the matrix. Unfortunately, fully conjugated polymers, as used for fluorescent LEDs, generally have a low energy triplet state,[11] which limits their utilization as host in PPLEDs. One way to circumvent this problem is the use of non-conjugated polymers, such as poly(N-vinylcarbazole) (PVK).[13–15] However, PVK exhibits rather poor electron transporting properties, and additional compounds, typically oxadiazole derivatives, need to be added to facilitate electron injection and transport. To avoid problems that may arise from phase separation in multi-component blends, non-conjugated copolymers containing hole and electron transporting moieties can provide ambipolar transport properties with an appropriate position of the triplet state.[16]

Recently, we presented a new series of polymer matrices for phosphorescent dopants, using a polystyrene backbone as a carrier for hole and electron transporting side-groups. These new materials lead to efficient PLEDs with low onset voltage.[17–19] In this paper, we present a new ambipolar matrix for phosphorescent PLEDs. We compare a random copolymer with a blend of homopolymers of the same monomers as matrix material in molecular doped PLEDs. To understand and optimize the device performance, detailed investigations of the dynamics of injection, transport, and recombination of charges have been performed. We find that the performance of the PLEDs is limited by the phosphorescence efficiency of the dye used, but is rather independent of whether the dye is added to a copolymer or a polymer blend.

a)Author to whom correspondence should be addressed. Electronic mail: neher@uni-potsdam.de.

II. EXPERIMENTAL

A 4,4,4″-tri(N-carbazo1yl)triphenylamine (TCTA)-analog monomer was used as the hole transporting component. As the electron transporting unit, a phenylbenzimidazole derivative was selected. The complete syntheses of both compounds and the polymerization conditions were recently described.[18,19] Both transporting units are attached at the 4-position to a styrene moiety. Polymerization, therefore, results in the formation of a polystyrene backbone, bearing the charge-transporting units as side groups. The chemical structures of the novel random copolymer and the homopolymers are depicted in Fig. 1, and the polymer properties are listed in Table I. The polymerizations were done by means of a free radical process. Freshly distilled tetrahydrofurane (THF) was used as a solvent, 2 mol.% N,N-Azo-bis-(isobutyronitrile) (AIBN) was used as initiator, and the polymerizations were performed in a glovebox system at 50 °C for 64 h. After that, the solutions were demonomerised by repeated precipitations of the polymers into mixtures of methanol and diethylether (2:1). The yields of all polymerizations are in the range of 80%. Gel permeation chromatography (GPC) was chosen to determine the molecular weight of the polymers using polystyrene calibration. For all polymers, relatively broad distributions were obtained. Since there were no additional peaks found in the ^{1}H and ^{13}C NMR spectra of the polymers, this phenomenon was not further investigated with regard to possible chain transfer reactions during polymerization. ^{13}C NMR spectroscopy was used to determine the copolymer composition. By comparing the C2 atom at the phenylbenzimidazole unit between the two N atoms in the electron transporting unit (151 ppm) and the signal of the C aromatics connected to the centered N-atom in the hole transporting monomer (146 ppm), the content of the hole and electron transporting units was calculated to be 38% and 62%, respectively. A 2:1 ratio of electron transporting units to hole transporting units was found to be optimal for this system in previous measurements and, therefore, the targeted copolymer composition. The phosphorescent dye used is an organo-metallic complex with iridium core provided by Merck KGaA.

PLED devices presented here were fabricated under nitrogen atmosphere on indium tin oxide (ITO) coated glass substrates coated with PEDOT:PSS (Clevios P VP AI4083, Heraeus Clevios GmbH). To improve hole injection into the active layer, a polymeric hole injection material provided by Merck KGaA was coated on PEDOT:PSS from toluene solution. Its HOMO and LUMO energies are about −5.1 eV and −1.9 eV, respectively. After that, the film was baked at 180 °C for 1 h. After that treatment, an insoluble "hole injecting interlayer" (HIL) of approximately 5 nm thickness was formed that remained on top of PEDOT:PSS after washing with organic solvents, such as chlorobenzene.[20–22] It was, however, found that the same device performance was achieved when coating the active layer on top of HIL without the additional washing step. The active layer was spin-coated from chlorobenzene solution on top of HIL and dried at 180 °C for 10 min. For a complete OLED, the active layer consisted either of the copolymer blended with 17 wt.% dye (type I) or a 2:1 blend of polymers **1** and **2** doped with 17 wt.% dye (type II). Cathode materials (CsF (1 nm), Ba (3 nm), or Sm (10 nm) covered by Al (150 nm)) were subsequently thermally evaporated in high vacuum at pressures of 10^{-6} mbar. The final device structure consists of ITO/PEDOT:PSS (60 nm)/HIL (5 nm)/matrix doped with phosphorescent dye (60 nm)/cathode, with an active area of 16 mm^2. Luminance-voltage and current-voltage characteristics were measured in a nitrogen atmosphere with a Konica Minolta CS-100 ChromaMeter and a Keithley 2400 SourceMeter.

Mobilities of electrons and holes in the active layer were measured by sensitized transient electroluminescence (TEL). A detailed description of this method is published elsewhere.[23] To measure electron mobility, the OLED device structure, as described above, was altered by replacing the HIL layer with an insoluble poly[2,5-dimethoxy-1,4-phenylene-1,2-ethenylene-2-methoxy-5-(2-ethylhexyloxy)-(1,4-phenylene-1,2-ethenylene)] (M3EH-PPV, H.-H. Hörhold, Jena) sensing layer of 5 nm

TABLE I. Polymer properties of polymer **1**, polymer **2**, and the copolymer.

Polymer		Polymer **1**	Polymer **2**	Copolymer
Yield in %		87	81	85
Content hole transporting unit[a]	In mol.%	100	0	38
Content electron transporting unit[a]	In mol.%	0	100	62
Molecular weight in 10^3 g/mol[b]	M_n	17.8	56.2	30.3
	M_w	66.5	275.0	128.9
	PDI[d]	3.36	4.89	4.25
T_g in °C[c]	T_g	244	224	231

[a]^{13}C NMR.
[b]GPC in THF at RT.
[c]DSC.
[d]Polydispersity index.

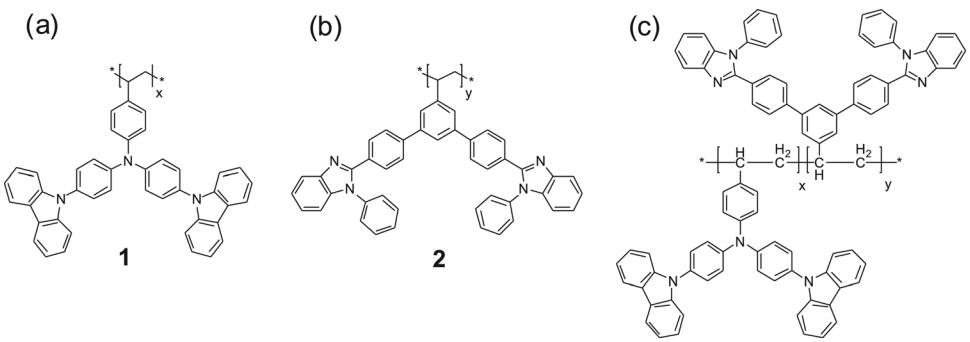

FIG. 1. Chemical structures of hole transporting polymer **1** (a), electron transporting polymer **2** (b), and the random copolymer (c).

thickness formed by the "interlayer method".[21,23] CsF covered by Al was used as the cathode. For hole mobility measurements, a red-emitting small molecule provided by Merck KGaA was evaporated as a sensing layer (10 nm) on top of the active layer stack. In this case, Ba and Al were evaporated as a cathode. All devices for TEL measurements had an active area of 2 mm^2. For TEL measurements, samples were encapsulated with a glass lid and electrically excited by a homemade function generator with 25 ns rise time (10%-90%). The light output was recorded by a monochromator and photomultiplier with time resolution below 15 ns.

Steady-state spectra of the electroluminescence (EL) were measured with an OceanOptics HR2000 spectrometer. Absorption and photoluminescence (PL) spectra were recorded using a Varian Cary 5000 spectrophotometer and a Horiba Jobin Yvon Fluorolog-3 spectrometer, respectively. External quantum efficiencies of the PLEDs were measured with a Gigahertz-Optik X4 Light Analyzer set-up, incorporating an integrating sphere. To prevent the edge-emitted light from reaching the detector, the PLED edges were masked with black paint. Absolute PL efficiencies were determined with a Hamamatsu C9920 setup, including an integrating sphere combined with a photonic multi-channel analyzer. Kinetic properties of the phosphorescent dye were investigated by excitation from an EKSPLA NT-242 Nd:YAG/optical parametric oscillator system with pulse widths below 6 ns. The transient decay of the phosphorescence was recorded by a monochromator and a Becker & Hickl multiscaler PMS 400.

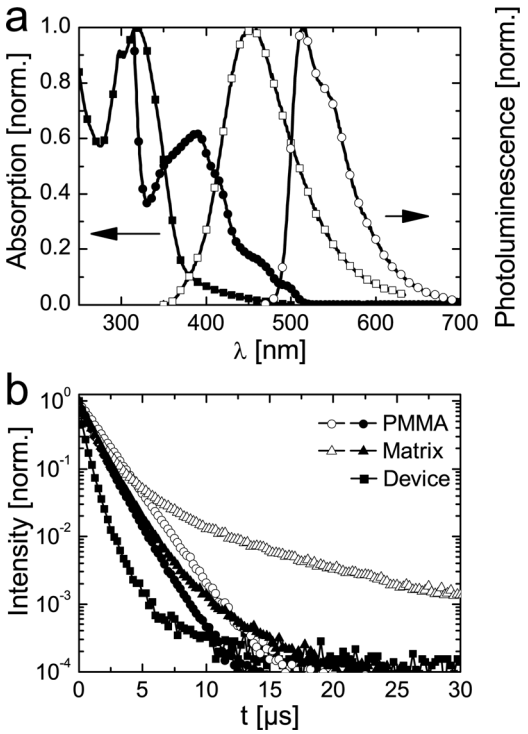

FIG. 2. (a) Absorption (closed symbols) and luminescence spectra (open symbols) for thin films of the copolymer (squares) and PMMA doped with 3 wt.% of phosphorescent dye (circles). (b) Decay of the dopant phosphorescence in PMMA (circles), in the copolymer (triangles) and in a full type I device (squares) at 300 K. Open symbols correspond to a dopant concentration of 3 wt.%, closed ones to 17 wt.%. The layer thickness is 70 nm and $\lambda_{exc} = 420$ nm.

III. RESULTS AND DISCUSSION

A. Electronic and optical properties

Positions of the highest occupied molecular orbital (HOMO) (−6.3 eV) and the lowest unoccupied molecular orbital (LUMO) (−2.0 eV) levels for the electron transporting polymer were estimated by cyclovoltammetry for a film on glass-carbon electrode against an Ag/AgCl reference. The optical bandgap calculated from UV/Vis data in $CHCl_3$ solution is 3.5 eV. The same method was used to determine the HOMO level position (−5.4 eV) and optical bandgap (3.3 eV) for the hole transporting polymer. The LUMO energy of the hole transporting homopolymer was not accessible by cyclovoltammetry and is therefore expected to be smaller than −2.0 eV. The measured HOMO and bandgap energies support this assumption. As the charge transporting moieties are attached to individual side groups of the copolymer, we expect that the copolymer has its HOMO at −5.4 eV and its LUMO at −2.0 eV.

Figure 2(a) presents absorption and fluorescence spectra of the copolymer film and the absorption and phosphorescence spectra of 3 wt.% dye in a PMMA matrix. The phosphorescent dye emits green light with CIE 1931 color coordinates of $x = 0.37$ and $y = 0.60$. When blended at 3 wt.% into PMMA, the dye phosphorescence decays monoexponentially with $\tau = 1.6$ μs (see Fig. 2(b)). At the excitation wavelength of 420 nm, only the phosphorescent dye is excited. With an optical density of approximately 0.015, excitation can be assumed to occur homogeneously throughout the film. The PL quantum yield is ca. 95% for a concentration of 3 wt.% in PMMA. Both observations indicate the almost complete lack of intramolecular nonradiative decay processes. On the other hand, a non-monoexponential decay is observed when the dye is blended with the copolymer, even for a low dye concentration. At short times, the phosphorescence decays significantly faster than in the PMMA matrix, while the decay gets much slower at longer times. Such decay characteristics can be explained by energy transfer between the triplet state of the dopant and an energetically close triplet state of the matrix.[24–26] This process results in a quenching of the primary dye excitation, as expressed by a shortening of its initial decay. Back transfer from the supposedly long-living triplet state of the matrix to the dopant produces the long-lived tail in the PL decay.[26,27] To identify the component which is mainly responsible for this effect, the phosphorescence decay of the dye was measured separately in the homopolymers **1** and **2**. In polymer **1**, a mono-exponential decay with $\tau = 1.2$ μs is observed, while the decay in polymer **2** is close to that observed in the copolymer. Apparently, the dye interacts strongly with the electron transporting component of the matrix, leading to the observed multiexponential decay. Interestingly, the quantum yield of the dye phosphorescence at a concentration of 3 wt.% is, within the reproducibility of the measurement, approximately the same (about 65%) in polymer **1**, polymer **2**, and the copolymer.

Increasing the dye concentration from 3 to 17 wt.% strongly influences the decay dynamics. In PMMA, an

increased dye concentration leads to an overall faster decay, which remains almost mono-exponential, accompanied by a slight drop in quantum yield. In the copolymer, the long-lived decay component is strongly reduced. At the same time, the quantum yield drops to 50% ± 5% in the copolymer. Both effects can be explained by a formation of non-emissive dye aggregates in the polymer matrix, which quench the dye emission due to a lower triplet energy.

B. PLED performance

Figure 3 presents current density – voltage and luminance – voltage characteristics for type I PLEDs using different cathode materials. For a given bias, the highest current and luminance is measured in PLEDs with a CsF/Al cathode, while the usage of Ba as a cathode material leads to almost 10 times lower values. Using a Sm cathode, the current decreases further, while the measured luminance drops by more than two orders of magnitude. Taking into account the LUMO position of the electron transporting moiety at −2.0 eV and the work functions of the used metals, the most efficient electron injection into the matrix is indeed expected from CsF/Al (Cs work function 2.1 eV), while the use of Ba (2.6 eV) and especially of Sm (2.7 eV) as cathode materials should result in significant energetic barriers for the injection of electrons into the active layer.

The current – voltage, luminance – voltage and efficiency – current density characteristics for type I and type II PLEDs comprising a CsF/Al cathode are shown in Fig. 4. The graphs demonstrate similar behavior for both types. The efficiencies (Fig. 4(b)) increase with increasing current up to a maximum, after which they decrease monotonically. Such effect can be caused by strong quenching (triplet-triplet annihilation (TTA) and/or triplet-polaron interaction) of the dopant phosphorescence at high triplet exciton densities that occur at high currents.[24] As the phosphorescence decay times decreased twofold when the excitation power was increased from 2 to 300 μJ/pulse, TTA seems to be the main reason for the efficiency roll-off.

We also investigated the effect of dopant concentration on the PLED performance (data not shown). Introduction of the dopant into the matrix at low concentration (up to ca. 5 wt.%) was accompanied by a decrease in the bipolar device

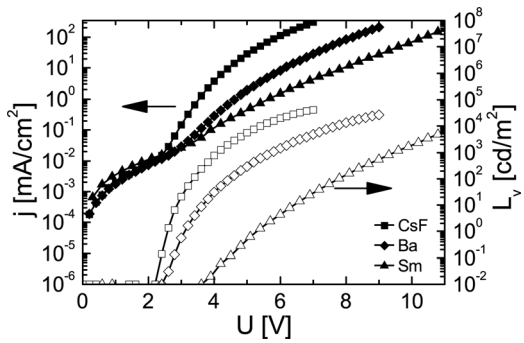

FIG. 3. Current-voltage (filled symbols) and luminance-voltage characteristics (open symbols) for type I PLEDs with an active layer of 60 nm thickness using CsF (squares), Ba (diamonds), or Sm (triangles) as cathode materials at $T = 296$ K.

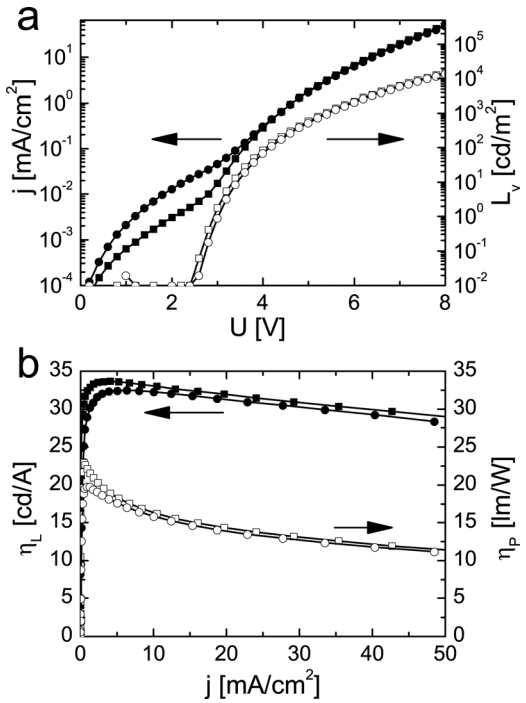

FIG. 4. (a) Current-voltage characteristics (closed symbols) and luminance-voltage curves (open symbols) for type I PLEDs with 75 nm active layer (squares) and type II PLEDs with 70 nm active layer thickness (circles) with CsF/Al cathode. (b) Corresponding dependencies of the luminous efficiency (η_L, closed symbols) and of the luminous power efficiency (η_P, open symbols) on the current.

current. This indicates that the dye molecules act as traps for the majority charge carriers. A further increase of the dye concentration up to 17 wt.% does not influence the current, which can be explained by the formation of a percolation subsystem for charge transport along the dopant molecules.[28] At the same time, the luminous efficiency and the luminous power efficiency rise monotonically with the dye concentration. The drop of efficiency observed at high current densities did not depend on the dye concentration. This situation is close to that observed for phosphorescent PLEDs based on small organic molecules[24] and PVK.[29] As shown in Ref. 29, the independence of the efficiency drop on dopant concentration indicates a strong contribution of triplet-triplet annihilation on the matrix that has a triplet energy similar to that of the dopant.

The dependence of the external EL quantum efficiency on the current follows the dependence of the luminous efficiency (displayed in Fig. 4(b)). A maximum quantum efficiency of 8–10% is measured in the range of 5–25 mA/cm^2. This value is close to the theoretical maximum achievable for the system under investigation, considering a PL quantum yield of 50% and a light out-coupling efficiency of 20% (for a glass substrate with index of refraction $n = 1.5$).[30]

C. Charge carrier mobilities

The charge carrier mobility of the system was investigated by TEL using thin sensing layers, as described in section II. The energy level diagram of the system used for electron mobility measurements is presented in Fig. 5(a).

The HIL was replaced by an insoluble M3EH-PPV sensing layer with 5 nm thickness. Since the sensing layer's HOMO energy level (−5.1 eV) is comparable to the work function of PEDOT:PSS and its LUMO energy level (−2.7 eV) is lower than in the polymer used, we expect efficient hole injection into M3EH-PPV from the anode, while electrons arriving at the active layer/M3EH-PPV interface can easily cross the interface, leading to orange emission from M3EH-PPV at 590 nm. Since light emission requires the recombination of electrons and holes, the sensing layer emission can be used to detect the arrival of electrons at the anode side of the device. The transient luminance of a copolymer device doped with 17 wt.% of phosphorescent dye as the active layer at different pulse voltages is presented in Fig. 5(b). With the TEL onset being determined by the transit of electrons through the emission layer, the electron mobility can be calculated according to $\mu = d_{\mathrm{EML}}/(t_{\mathrm{d}}\, E)$. Here, we have used the TEL time delay, t_{d}, defined by the linear extrapolation of the initial EL rise toward zero brightness (see straight lines in Fig. 5(b)) to determine the mobility. d_{EML} is the thickness of the active layer, $E = (U - U_{\mathrm{bi}})/d_{\mathrm{total}}$ is the internal electric field strength at the applied voltage U, U_{bi} is the built-in potential due to the electrode work function difference, and d_{total} is the thickness of the full polymer stack, namely the active layer plus sensing layer. Note that hole injection into the active layer is also possible, due to the close proximity of the HOMO levels of the sensing layer and hole conducting components in the EML. Investigation of the steady-state EL spectra of the TEL device with a M3EH-PPVsensing layer and a dye-doped EML clearly shows emission contributions from both the sensing layer and the phosphorescent dye at higher bias, while pure M3EH-PPV luminescence in the device with a doped matrix is observed only at low bias. In the former case, M3EH-PPV emission can arise both from electron-hole recombination in the sensing layer and energy transfer from excitons formed in the matrix to M3EH-PPV. This might overestimate the mobility with the method described above. Another important issue is that hole injection into the active layer makes the device bipolar. It was theoretically shown that the mobility of charge carriers in unipolar and bipolar devices may be different.[31] To analyze this point, we compared TEL registered at 590 nm (sensing layer fluorescence) and 520 nm (dopant phosphorescence). As shown in Fig. 5(b), green emission sets in after the red emission. Apparently, hole injection from the sensing layer into the active layer occurs only after the arrival of electrons at the interface. Therefore, the mobilities extracted from the sensitized TEL measurements can reliably be assigned to electrons traversing the active layer.

The so-determined electron mobilities are presented in Fig. 6 for the different polymeric matrices. The field dependence of the mobility approximately follows a Poole-Frenkel dependence $\mu \propto \exp\{\beta\sqrt{E}\}$. Noticeably, the mobility is almost the same for the electron transporting polymer **2** and the copolymer, while it is slightly smaller for the blend of the two homopolymers **1** and **2**. Addition of the dye decreases the electron mobility in both the copolymer and the blend matrix, though the reduction is more pronounced for the blend system. This difference might be caused by different morphologies of both matrices. The mobility decrease supports our conclusion made above that dye molecules act as traps.

An energy level diagram of the system used for hole mobility measurements is shown in Fig. 7(a). The LUMO level of the sensing layer (−3.3 eV) provides effective injection of electrons from the Ba cathode used. At the same time, a high barrier at the interface between the sensing layer and the EML leads to a confinement of electrons in the sensing layer. The HOMO level of the sensing layer (−5.6 eV) matches well to the HOMO level of the hole conducting component of the matrix, facilitating hole injection from the matrix into the sensing layer. Therefore, the onset of

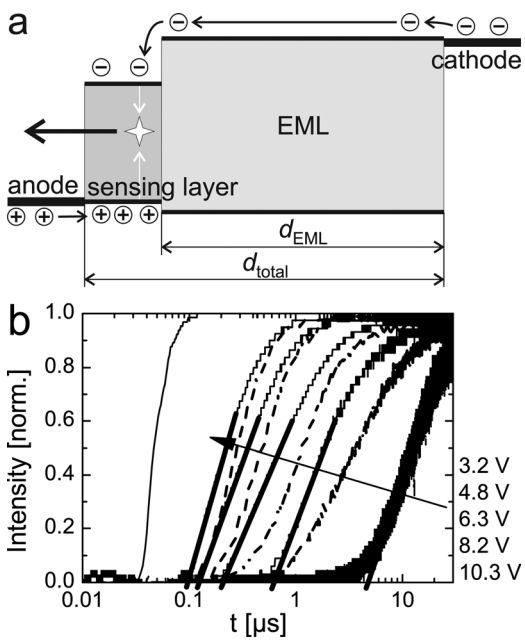

FIG. 5. (a) Scheme of the layer stack and energy levels for the electron conductivity measurement by TEL. (b) Transient luminance from devices with M3EH-PPV sensing layer (5 nm) and type I active layer (60 nm) at different pulse voltages. Solid curves were recorded at a wavelength of 590 nm (sensing layer emission) and dashed ones at a wavelength of 520 nm (active layer emission). The luminance curves have been normalized to their respective maximum. The solid line at short times is the measured voltage ramp.

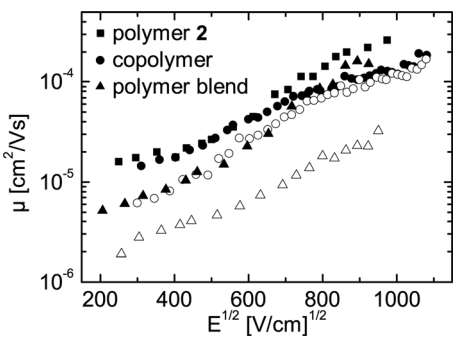

FIG. 6. Electron mobilities for devices with different active layer compositions calculated from TEL delay times. Squares, circles, and triangles denote polymer **2**, copolymer, and the polymer blend, respectively. Filled symbols correspond to undoped layers; open ones correspond to layers doped with 17 wt.% phosphorescent dye.

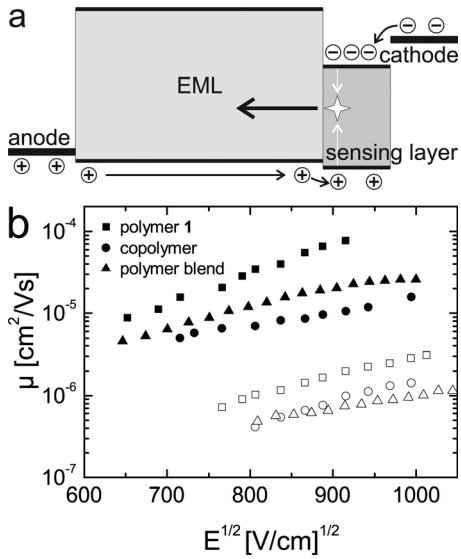

FIG. 7. (a) Scheme of the layer stack and energy levels for the hole mobility measurements by TEL. (b) Hole mobilities for the devices with different active layers calculated from TEL delay times. Squares, circles, and triangles denote polymer **1**, copolymer, and the polymer blend, respectively. Filled symbols correspond to undoped layers; open ones correspond to layers doped with 17 wt.% dye.

emission from the sensing layer in TEL is a good measure for the transit time of holes through the active layer. Figure 7(b) shows the hole mobilities in the copolymer and the hole transporting homopolymer. The hole mobility in the pure hole transporting polymer **1** is about 10^{-5}–10^{-4} cm^2/Vs, and it is decreased upon addition of the electron transporting moieties either within the same chain (copolymer) or in the blend with polymer **2**. This is attributed to the dilution of hole transporting sites by the electron transporting component of the films that has a two times higher concentration.

In both the copolymer and the blend, the mobility of electrons is about an order of magnitude larger than the hole mobility, pointing to imbalanced transport properties. This imbalance becomes even more pronounced upon addition of the phosphorescent dye, which reduces the hole mobility to ca. 10^{-6} cm^2/Vs in both the copolymer and the blend. Again, the effect is more pronounced for the blend film. Clearly, dye molecules trap both types of charge carries in the system under investigation. In both systems, electron mobilities are almost two orders of magnitude higher than hole mobilities, although the mobilities are slightly more balanced in the polymer blend system.

According to the measured mobilities, the onset of the bipolar full device should be determined by the motion of electrons through the active layer. Figure 8 compares the transient EL measured at 520 nm of a single layer device with the TEL at 590 nm for a bilayer stack comprising a M3EH-PPV sensing layer. The transient behavior of the single layer device closely follows the kinetics of the emission from the electron sensing layer. Apparently, the motion of electrons is the time-limiting process, while injection of holes into the active layer does not cause an additional time delay. The data also suggests that the recombination zone is close to the anode.

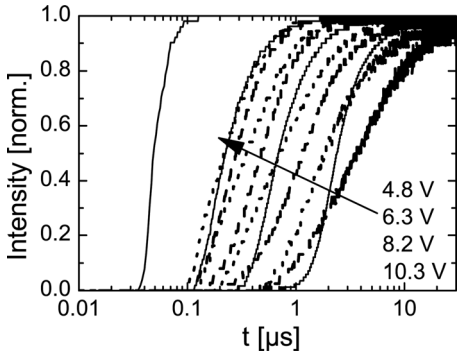

FIG. 8. Transient luminance of full type I devices (solid lines) and of devices with M3EH-PPV sensing layer (dashed lines) (active layer thickness 60 nm) at different pulse voltages recorded at a wavelength of 520 nm. Dotted lines mark transient luminance from the devices with M3EH-PPV sensing layer recorded at a wavelength of 590 nm. The luminance curves have been normalized to their respective maximum.

IV. EVALUATION OF THE DEVICE PERFORMANCE

The analysis of charge transport, as described above in Subsection III C, suggests a large imbalance of electron and hole transport. On the other hand, maximum internal quantum efficiencies (calculated from the external EL quantum efficiency, assuming an outcoupling efficiency of 20%) are about 40–50%, close to the PL quantum efficiency of the dye-doped polymer systems at a dye concentration of 17 wt.%. This suggests that the flow of electrons and holes into the device and their recombination within the active layer is not solely determined by the carrier mobilities. This conclusion is further supported by the rather similar device properties of type I and II devices, despite the significantly lower electron mobility in the dye-doped polymer blend (type II). In Subsections IV A–IV C, a description of processes determining the performance of the devices is given.

A. Charge injection in unipolar and bipolar devices

To investigate the efficiency for charge injection, unipolar devices were constructed in which one electrode was chosen as in the bipolar device, and the other was to block injection of carriers of the opposite sign. Devices with different active layer thicknesses were built for both the blend and the copolymer system, with and without dye. Selected results are summarized in Fig. 9. Also included are space-charge limited currents calculated by the Mott-Guerney law using the mobilities determined by TEL, as described above.

For hole-only devices, the cathode was replaced by MoO_3. This metal oxide has gained much attention due to its rather high work function, which makes it a good hole injector.[32,33] None of the devices with MoO_3 showed detectable light emission, indicating truly unipolar current flow. Obviously, the measured hole-only currents are orders of magnitude lower than the theoretical space charge limited maximum for both the undoped and the dye-doped films. Also, the hole-only currents measured for devices with different thickness fell on the same line when plotted as a function of electric field (Fig. 10). This indicates injection-

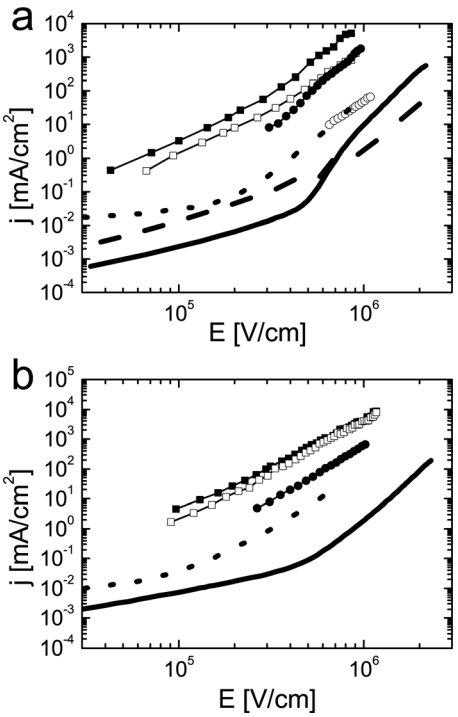

FIG. 9. Current density as a function of applied electric field for a series of blend (a) and copolymer (b) devices. Filled (open) squares indicate calculated electron space charge limited current (SCLC) without (with) dye; filled (open) circles calculated hole SCLC without (with) dye; full (dashed) line measured hole-only currents without (with) dye; and dotted line bipolar currents in full devices with dye. All blend layers were about 65 nm thick; all copolymer films about 90 nm. The measured bipolar characteristics were corrected for a built-in field of 2.6 V determined by taking into account the work function difference of the electrodes as measured by Kelvin probe. The build-in voltage of the hole-only devices was taken to be zero due to Fermi-level pinning at both contacts determined by Kelvin probe measurements.

limited hole currents for all devices. Experiments on hole-only devices without and with the HIL on top of PEDOT:PSS clearly indicated that HIL promotes hole injection (Fig. 11). In accordance to this finding, bipolar devices without the HIL interlayer exhibited much lower performances (not shown here). Upon dye addition, there is little change in the hole-only currents, despite the fact that the hole mobility decreases significantly. The main effect of

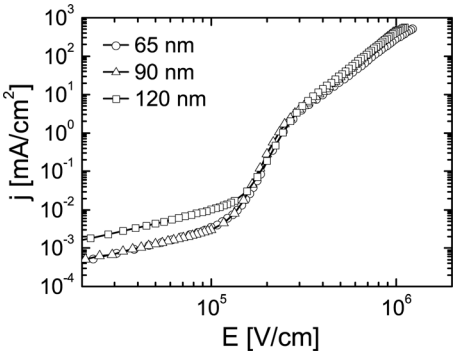

FIG. 10. Current-voltage characteristics of hole-only devices of polymer **1** with different active layer thicknesses of 65 nm (circles), 90 nm (triangles), and 120 nm (squares). The device structure is PEDOT:PSS/HIL/polymer 1/MoO_3 (20 nm)/Al.

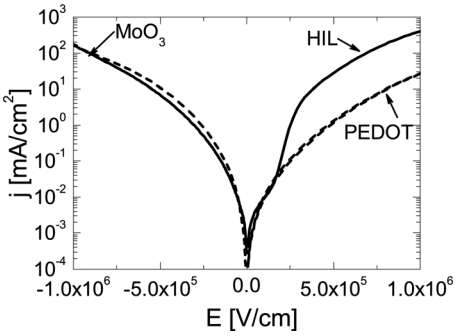

FIG. 11. Current-voltage characteristics for hole-only devices of polymer **1** with (solid line) and without (dashed line) HIL. The thickness of the polymer layer was 90 nm. The injecting contact is indicated in the figure.

adding the dye is a less defined current turn-on. The currents are quite similar for both blend and copolymer films, with slightly higher currents in the blend. Most likely, the dye constitutes an additional channel for more efficient injection, while it also reduces the current through the bulk of the layer.

The construction of electron-only unipolar devices proved to be more complicated. The use of aluminum cathodes, following the procedure in Ref. 34, resulted in high leakage currents and devices with low reproducibility. We also built "quasi electron-only devices" by replacing the HIL with an interlayer from poly(3-hexylthiophene) (P3HT).[35] However, only a limited field range was accessible for these devices, as hole injection through the P3HT occurred at higher fields (indicated by the onset of detectable light emission). Also, the reproducibility of these devices was still poor. Therefore, we were unable to access the efficiency of electron injection in these devices.

Also included in Fig. 9 are characteristics of bipolar devices. These currents are significantly higher than for the hole-only devices. Since the high EL efficiency of the bipolar devices suggests efficient recombination of all electrons and holes, the current in the bipolar device is roughly equal to the flow of holes into the active layer. Therefore, hole injection must be largely enhanced in the working OLED when compared to the respective hole-only device. A possible scenario is that electrons are accumulated at the interlayer, leading to a significant enhancement of the electric field across the interlayer, which improves hole injection.[22,36] In the ideal case of perfect blocking of electron flow through the interlayer, this scenario will lead to a self-regulation of hole injection and electron recombination, resulting in an almost complete recombination of all charges close to the anode. This interpretation is further supported by our observations in TEL, as described above. For electron mobility measurements, we replaced HIL by the emissive M3EH-PPV, which has a HOMO energy similar to HIL. We observed hole injection, indicated by EML emission, only after the arrival of electrons at the PPV/EML interface, indicated by the earlier onset of sensing layer emission. As the LUMO of HIL marks a barrier for electron extraction from the EML, the accumulation of electrons, which in turn improves hole injection into the EML, seems likely.

B. Cathode quenching

The data presented so far suggests that the recombination zone is located close to the HIL/EML interface. This conclusion is supported by an investigation of device phosphorescence decay under photoexcitation. As shown in Fig. 2(b), the phosphorescence in the device (comprising the electrodes) decays significantly faster than in the same layer coated onto a bare glass substrate, indicating electrode-induced excitation quenching. Note that photoexcitation was at 420 nm. At this wavelength, light is absorbed almost homogeneously through the whole layer thickness. To identify which electrode is responsible for this quenching, the phosphorescence decay was measured for two different sample geometries. The first one comprises the active layer on top of ITO/PEDOT:PSS/HIL, but without the top electrode. In this case, the decay dynamics were almost identical to those of the active layer directly on glass. Contrary to that, when the active layer was deposited on bare glass and covered by a CsF/Al electrode, the phosphorescence decay was close to what is observed in the full device. We also found that the phosphorescent decay rate increases with decreasing active layer thickness. This result shows that the quenching of the photo-induced dye phosphorescence, as observed in the full device, is due to non-radiative interactions with the cathode metal.[37,38] This quenching leads to a decrease of the dye's PL quantum yield to 20–25%. To check how the distance between the metal and the phosphorescent dyes affects the decay rate, films of dicarbazole-biphenyl (CBP) with variable thickness were inserted between a ca. 20 nm thick active layer and the cathode. Figure 12 presents the PL decay curves for different thicknesses of the CBP spacer. Clearly, quenching becomes weaker with increasing thickness of the CBP layer, and it is insignificant at spacer thicknesses higher than ca. 70 nm.

The rather high EL efficiency of the dye-doped polymer systems suggests that cathode-induced quenching of the excitons generated on the phosphorescent dye by charge recombination must be rather small. We therefore conclude that most of the emissive excitons are generated in close proximity to the anode.

C. Space charge effects

According to Fig. 9, the currents of the bipolar devices are significantly smaller than the predicted space-charge limited electron currents. As pointed out above, we expect that electrons are effectively blocked at the interlayer, but other effects, such as hindered electron injection (due to injection barriers or oxides formed at the cathode), might be the reason for the smaller bipolar device current.

Interestingly, we found that the bias between the voltage pulses in the TEL experiments on bipolar devices had a significant effect on the EL intensity during pulsed operation. As shown in Fig. 13(a), changing the bias value from +2.24 V (close to flat-band) to −7 V (high reverse bias) led to a twofold increase in TEL intensity. This effect can be explained by the presence of traps in the active layer. Charges that are injected and trapped during device operation will form a space charge in the film, which counteracts the applied voltage. If a positive bias close to the built-in voltage is applied between the voltage pulses, charges remain in the traps during the time between the voltage pulses. This space charge impedes the injection of additional charge carriers into the active layer. Application of a large

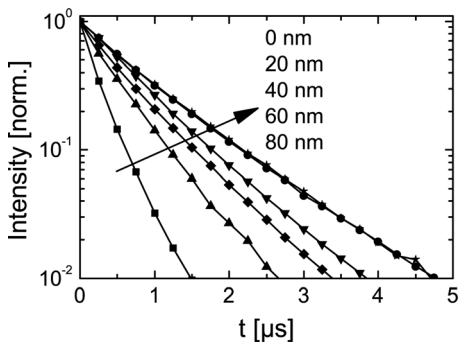

FIG. 12. Decay of the dopant phosphorescence in devices with 20 nm type II layer for different CBP thicknesses as indicated in the figure; $\lambda_{exc} = 420$ nm. Stars mark the decay of a film without a spacer and cathode.

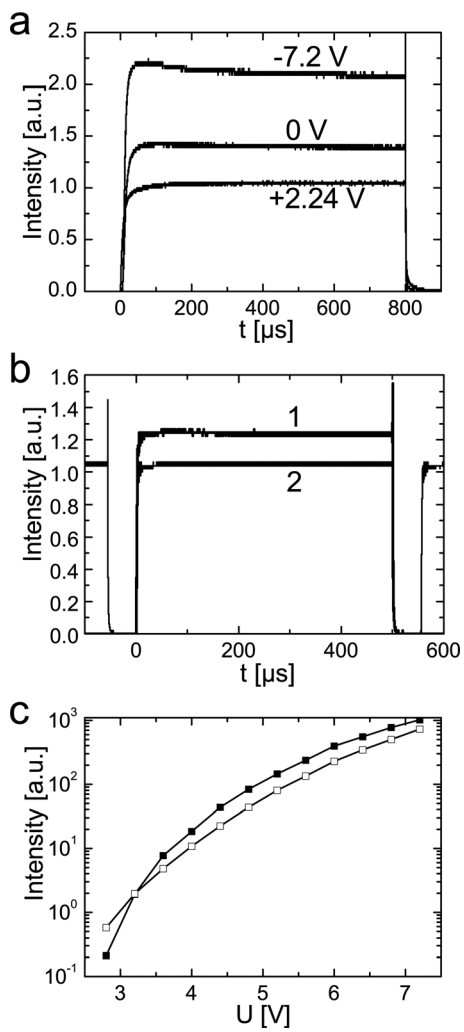

FIG. 13. (a) Transient luminance of type II devices (60 nm) at different biases between the voltage pulses for a constant pulse voltage of 4 V. (b) TEL for different duty cycles; transient 1 corresponds to 15% and transient 2 to 90% for a pulse voltage of 8 V and a bias of 0 V. (c) Dependence of the value of TEL maximum on the pulse voltage for a duty cycle of 15% and bias of −8 V (filled squares) and a duty cycle of 90% and 0 V bias (open squares).

negative bias between pulses apparently removes the trapped charges from the device, which allows efficient charge injection at the beginning of the next pulse (indicated by the observed TEL overshoot) and an overall higher EL intensity.

If the scenario described above is true, the TEL intensity should be sensitive to the duty cycle. This is expected because detrapping of charges requires a certain time. In accordance to this, we found the TEL intensity to decrease monotonically with duty cycle above a duty cycle of 40%. Figure 13(b) shows two example transients.

Figure 13(c) presents dependencies of the TEL amplitude on the voltage during operation for a duty cycle of 15% and a negative bias applied between pulses (full squares) and for a duty cycle of 90% with zero bias between pulses (open squares). The latter case closely represents the device under steady state operation. The TEL intensity is almost two times higher for negative bias and small duty cycle, indicating that the EL emission intensity of the operating device at a given voltage is significantly reduced by the build-up of space charge.

V. CONCLUSIONS

We have shown detailed investigations of electrophosphorescent OLEDs based on a charge-transporting polymer matrix doped with a green phosphorescent dye. The devices show an external EL quantum efficiency of 8–10%, close to what can be expected regarding the dye's PL quantum efficiency of about 50%. At the same time, the measured mobilities of electrons is at least one order of magnitude higher than the hole mobility. This on its own should lead to a much lower device efficiency. However, the devices show injection-limited hole currents in unipolar devices. Apparently, the accumulation of electrons at the hole injecting interface of the bipolar devices leads to an efficient and self-balanced hole injection. The injected holes have a rather low mobility and encounter a large space charge of electrons, which results in recombination and light emission close to the anode. This in turn prevents undesired luminescence quenching by interactions with the cathode metals. The formation of space charges is demonstrated by the device behavior under pulsed operation at different pre-biases and duty cycles.

ACKNOWLEDGMENTS

We gratefully acknowledge the financial support from the Bundesministerium für Bildung und Forschung (BMBF projects "CARO", FKZ 01EBD0685 and "NEMO", FKZ 13N10618 and 13N10622). We also thank Merck KGaA for supplying the phosphorescent dye, the hole injecting interlayer, and sensing layer materials.

[1]R. H. Friend, R. W. Gymer, A. B. Holmes, J. H. Burroughes, R. N. Marks, C. Taliani, D. D. C. Bradley, D. A. Dos Santos, J.-L. Brédas, M. Lögdlund, and W. R. Salaneck, Nature **397**, 121 (1999).
[2]M. A. Baldo, D. F. O'Brien, M. E. Thompson, and S. R. Forrest, Phys. Rev. B **60**, 14422 (1999).
[3]J. Kido, H. Hayase, K. Hongawa, K. Nagai, and K. Okuyama, Appl. Phys. Lett. **65**, 2124 (1994).
[4]X. Zhang, R. Sun, Q. Zheng, T. Kobayashi, and W. Li, Appl. Phys. Lett. **71**, 2596 (1997).
[5]M. A. Baldo, D. F. O'Brien, Y. You, A. Shoustikov, S. Sibley, M. E. Thompson, and S. R. Forrest, Nature **395**, 151 (1998).
[6]M. A. Baldo, M. E. Thompson, and S. R. Forrest, Nature **403**, 750 (2000).
[7]V. Cleave, G. Yahioglu, P. Le Barny, R. H. Friend, and N. Tessler, Adv. Mater. **11**, 285 (1999).
[8]P. A. Lane, L. C. Palilis, D. F. O'Brien, C. Giebeler, A. J. Cadby, D. G. Lidzey, A. J. Campbell, W. Blau, and D. D. C. Bradley, Phys. Rev. B **63**, 235206 (2001).
[9]H. J. Su, F. I. Wu, C. F. Shu, Y. L. Tung, C. Yun, and G. H. Lee, J. Polym. Sci. A **43**, 859 (2005).
[10]X. H. Yang, D. Neher, U. Scherf, S. A. Bagnich, and H. Bässler, J. Appl. Phys. **93**, 4413 (2003).
[11]A. Köhler, J. S. Wilson, R. H. Friend, M. K. Al-Suti, M. S. Khan, A. Gerhard, and H. Bässler, J. Chem. Phys. **116**, 9457 (2002).
[12]J. W. Levell, J. P. Gunning, P. L. Burn, J. Robertson, and I. D. W. Samuel, Org. Electron. **11**, 1561 (2010).
[13]J. Kido, H. Shionoya, and K. Nagai, Appl. Phys. Lett. **67**, 2281 (1995).
[14]S. Lamansky, P. I. Djurovich, F. Abdel-Razzaq, S. Garon, D. L. Murphy, and M. E. Thompson, J. Appl. Phys. **92**, 1570 (2002).
[15]M. J. Yang and T. Tsutsui, Jpn. J. Appl. Phys. **39**, L828 (2000).
[16]M. Suzuki, S. Tokito, F. Sato, T. Igarashi, K. Kondo, T. Koyama, and T. Yamaguchi, Appl. Phys. Lett. **86**, 103507 (2005).
[17]M. Debeaux, M. W. Thesen, D. Schneidenbach, H. Hopf, S. Janietz, H. Krüger, A. Wedel, W. Kowalsky, and H. H. Johannes, Adv. Funct. Mater. **20**, 399 (2010).
[18]M. W. Thesen, B. Höfer, M. Debeaux, S. Janietz, A. Wedel, A. Köhler, H. H. Johannes, and H. Krüger, J. Polym. Sci. A **48**, 3417 (2010).
[19]M. W. Thesen, H. Krueger, S. Janietz, A. Wedel, and M. Graf, J. Polym. Sci. A **48**, 389 (2010).
[20]L. Duan, B. D. Chin, N. C. Yang, M.-H. Kim, H. D. Kim, S. T. Lee, and H. K. Chung, Synth. Met. **157**, 343 (2007).
[21]J. S. Kim, R. H. Friend, I. Grizzi, and J. H. Burroughes, Appl. Phys. Lett. **87**, 023506 (2005).
[22]X. Yang, F. Jaiser, B. Stiller, D. Neher, F. Galbrecht, and U. Scherf, Adv. Funct. Mater. **16**, 2156 (2006).
[23]S. Bange, A. Kuksov, and D. Neher, Appl. Phys. Lett. **91**, 143516 (2007).
[24]M. A. Baldo, C. Adachi, and S. R. Forrest, Phys. Rev. B **62**, 10967 (2000).
[25]J. Kalinowski, W. Stampor, M. Cocchi, D. Virgili, V. Fattori, and P. Di Marco, Chem. Phys. **297**, 39 (2004).
[26]X. H. Yang, F. Jaiser, S. Klinger, and D. Neher, Appl. Phys. Lett. **88**, 021107 (2006).
[27]K. Goushi, R. Kwong, J. J. Brown, H. Sasabe, and C. Adachi, J. Appl. Phys. **95**, 7798 (2004).
[28]D. M. Pai, J. F. Yanus, and M. Stolka, J. Phys. Chem. **88**, 4714 (1984).
[29]S. Lamansky, R. C. Kwong, M. Nugent, P. I. Djurovich, and M. E. Thompson, Org. Electron. **2**, 53 (2001).
[30]N. C. Greenham, R. H. Friend, and D. D. C. Bradley, Adv. Mater. **6**, 491 (1994).
[31]J. J. M. van der Holst, F. W. A. van Oost, R. Coehoorn, and P. A. Bobbert, Phys. Rev. B **80**, 235202 (2009).
[32]M. Kröger, S. Hamwi, J. Meyer, T. Riedl, W. Kowalsky, and A. Kahn, Appl. Phys. Lett. **95**, 123301 (2009).
[33]H. T. Nicolai, G. A. H. Wetzelaer, M. Kuik, A. J. Kronemeijer, B. de Boer, and P. W. M. Blom, Appl. Phys. Lett. **96**, 172107 (2010).
[34]R. Steyrleuthner, S. Bange, and D. Neher, J. Appl. Phys. **105**, 064509 (2009).
[35]S. Bange, A. Kuksov, D. Neher, A. Vollmer, N. Koch, A. Ludemann, and S. Heun, J. Appl. Phys. **104**, 104506 (2008).
[36]M. Gather, R. Jin, J. de Mello, D. Bradley, and K. Meerholz, Appl. Phys. B **95**, 113 (2009).
[37]H. Becker, S. E. Burns, and R. H. Friend, Phys. Rev. B **56**, 1893 (1997).
[38]V. Bulovic, V. B. Khalfin, G. Gu, P. E. Burrows, D. Z. Garbuzov, and S. R. Forrest, Phys. Rev. B **58**, 3730 (1998).